Autonomous Environment Disinfection Based on Dynamic UV-C Irradiation Map

Mathias Mantelli ⬡, Letícia dos Santos ⬡, Lucas de Fraga, Giovanna Miotto ⬡, Augusto Bergamin, Etevaldo Cardoso, Miguel Serrano, Renan Maffei ⬡, *Member, IEEE*, Edson Prestes, João Netto, and Mariana Kolberg ⬡, *Member, IEEE*

Abstract—The COVID-19 pandemic has become a worldwide concern and has motivated the entire scientific community to join efforts to fight it. Studies have shown that SARS-CoV-2 remains viable onsurfaces for days, increasing the chances of human infection. Environmental disinfection is thus an important action to prevent the transmission of the virus. Despite the valuable contribution of the research community to the field of UV-C disinfection by robots, there still lacks a disinfection system that is fully autonomous and computes its trajectory in real-time and in unknown environments. To meet this need, we propose an autonomous UV-C disinfection strategy for indoor environments based on a dynamic Irradiation Map that indicates the amount of energy applied in each region. Our method was tested in different scenarios and compared with other disinfection strategies. Experiments show that our approach delivers better results, especially when targeting high ideal UV-C doses.

Index Terms—Motion and path planning, service robotics, mapping, autonomous agents.

I. INTRODUCTION

THE Severe Acute Respiratory Syndrome Coronavirus 2 (SARS-CoV-2) has quickly and widely spread across many countries, threatening humans worldwide [1]. Studies have shown that SARS-CoV-2 remains viable on surfaces for days, which increases the chances of human infection [2], [3]. Researchers have also found SARS-CoV-2 present on surfaces within hospitals treating patients with COVID-19, indicating that the surfaces of environments should also be sanitized [4], [5]. Therefore, effective virus prevention should include environmental disinfection, in addition to other recommended practices like wearing masks and social distancing.

Mathias Mantelli, Letícia dos Santos, Lucas de Fraga, Giovanna Miotto, Renan Maffei, Edson Prestes, João Netto, and Mariana Kolberg are with the Institute of Informatics, Universidade Federal do Rio Grande do Sul, Porto Alegre 90650-001, Brazil (e-mail: mathiasfassini@gmail.com; lsantos@inf.ufrgs.br; lucas.fraga@inf.ufrgs.br; giovanna.lazzari.miotto@gmail.com; rqmaffei@gmail.com; prestes@inf.ufrgs.br; netto@inf.ufrgs.br; mariana.kolberg@inf.ufrgs.br).

Augusto Bergamin, Etevaldo Cardoso, and Miguel Serrano are with the Instor Robotics and Projects, 94410-970 Porto Alegre, Brazil (e-mail: augusto@instor.com.br; teo@instor.com.br; miguel@instor.com.br).

The research community has already studied the problem of preventing or reducing the spreading of viruses and other microorganisms, in which the ultraviolet type-C (UV-C) irradiation has been tested [6], [7]. The outcome was that the addition of a UV-C device significantly reduced the incidence of microorganisms, proving to be a suitable no-touch disinfection method. Since the SARS-CoV-2 outbreak, using UV lights in hospitals and other health centers has increased due to their effectiveness in environmental disinfection.

UV lights are a suitable candidate for environmental disinfection because their wide range of incidence quickly sanitizes the air and nearby surfaces while saving on water. Despite these advantages, long-time exposure to UV light is harmful to human skin and eyes [8]. In view of such a critical issue, attaching UV emitters to an autonomous unmanned ground vehicle (UGV) seems an appropriate solution that combines UV efficiency and human safety.

The research community has considered the idea of combining UV lights with autonomous robots. Tiseni *et al.* proposed a trajectory planner based on genetic algorithms (GA) that explores possible trajectories aiming to maximize the delivered UV dose [10]. Based on the irradiation physics and robot motion, their GA algorithm computes the best feasible disinfection trajectory. However, due to the high computational cost of their system, the calculation is wholly performed offline, based on the environment map that is known in advance, and then the disinfection trajectory is executed by the robot. Chanprakon *et al.* proposed a UV robot embedded with a Raspberry Pi for navigating through the environment, avoiding obstacles [11]. The authors mention that the robot can either be teleoperated or move autonomously. However, their autonomous mode does not compute a disinfection trajectory. Instead, it just avoids obstacles using a set of ultrasonic sensors on every robot's side, which means the robot's path for disinfection is not necessarily the most efficient. In contrast to the tower-shaped robots proposed by the two aforementioned papers, Conte *et al.* proposed a rectangular-shaped robot equipped with an arm [12]. Their robot is encircled with short UV lights, in combination with another UV light at the arm's end-effector. The main advantage of the arm is the six degrees of freedom, which allows the robot to disinfect a wide range of surfaces. Besides the robot, the authors also proposed a 3D gridmap for disinfection that determines the UV-C dose projected onto the environment's surfaces. A human teleoperates the robot during the disinfection process, moving
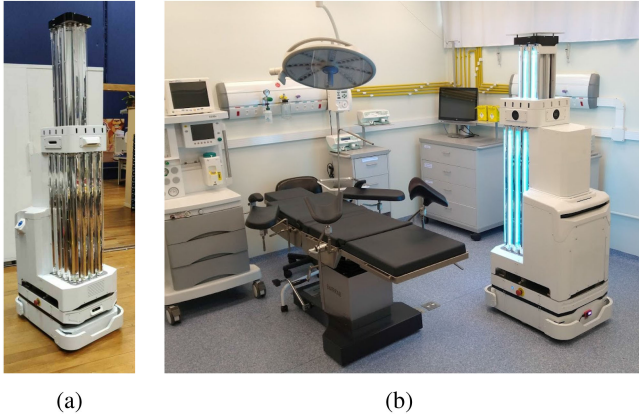
Fig. 1. Jaci is a disinfection robot developed by Instor [9], embedded with 18 UV-C lights in two different layers. (a) Jaci with the lights off. (b) Jaci in operation, disinfecting a hospital room.

the robot as the disinfection map indicates there is enough UV-C dose at the current surface.

Despite the valuable contribution of the research community to the field of UV-C disinfection by robots, there is still room for improvement. To the best of our knowledge, no work proposes a UV-C disinfection system that is fully autonomous, does not need any sort of pre-processing, and computes the disinfection trajectory on the fly on previously unknown environments. We propose a disinfection trajectory planner that performs its computation as the robot moves through the environment and builds an efficient 2D Irradiation Map describing the UV-C dose applied in the space. Our planner is based on a wall follower strategy, focusing on disinfecting the borders of obstacles and avoiding wide empty spaces to minimize the disinfection time. We evaluate our proposal withsimulated experiments, using the Jaci disinfection robot (Fig. 1). The results show that, differently from other tested approaches, our technique can adapt well to disinfect environments considering different levels of UV-C ideal dose.

This letter is organized as follows. Section II presents our irradiation map and how it is computed. This map is used by our autonomous disinfection planner, which is explained in Section III. The experiments in Section IV aim to validate our proposal and show the performance of our method in comparison with other disinfection planners. Section V concludes this work with an analysis of our findings and future goals.

II. IRRADIATION MAP

A. UV Irradiation Model

The UV spectrum ranges from 100 to 400 nm. It is subdivided into three types, type C containing wavelengths between 100 and 280 nm. UV-C is considered the most germicidal wavelength because the radiation is absorbed by the DNA and RNA of microorganisms, which breaks down their outer membrane [11], [12]. For every microorganism there is a specific amount of UV-C, called the ideal dose, which inactivates it.

To deliver a UV dose ξ, it is necessary to compute the radiant intensity of the lights and the exposure time. A light source

emits a radiant flux ϕ_e, and its radiant intensity I_e describes the released UV sterilization flow per solid angle Ω, i.e the angle into which the light is emitted. If we consider a punctual source of light, the irradiation happens in all directions of a sphere, then

$$I_e = \frac{\partial \phi_e}{\partial \Omega} = \frac{\phi_e}{4\pi}. \quad (1)$$

The irradiance E_e is the total irradiation incident at a surface with area A, and it is computed in terms of the radiant intensity as

$$E_e = \frac{\partial \phi_e}{\partial A} = \eta \frac{I_e}{|\vec{r}|^2}, \quad (2)$$

in which $|\vec{r}|$ is the distance between the light source and the surface, and $\eta = \cos \alpha$ is the optical efficiency impacted by the angle α between the vector $\vec{r}$ and the surface's normal $\vec{n}$.

The dose ξ delivered over a time period $\Delta t = t_i - t_{i-1}$, is computed as

$$\xi = \int_{t_{i-1}}^{t_i} E_e \, dt. \quad (3)$$

Assuming a static environment during such a period, E_e becomes a constant, and (3) can be rewritten as

$$\xi = E_e \Delta t = \eta \frac{\phi_e}{4\pi} \frac{\Delta t}{|\vec{r}|^2}. \quad (4)$$

Nevertheless, using a point light representation is usually a good approximation only when the distance between the lamp and the surface is not comparable to the size of the lamp itself. In the case of UV-C disinfection, due to the proximity to obstacles, the variation in $|\vec{r}|$ and η can considerably impact the results. Thus, given a lamp of size L and power P, we can compute ξ more accurately by integrating the irradiation caused by all lamp segments of size dL and power P/L.

B. The Irradiation 2D Gridmap

Our Irradiation Map is a 2D gridmap computed at a specific height of the environment. It uses as a basis a 2D occupancy gridmap and updates the UV-C irradiation on free-space cells that are visible from the robot pose. For simplification, all obstacles are considered like walls (with horizontal surface normals), while the cells in free-space are associated with vertical surface normals, as shown in Fig. 2.

The choice for a 2D irradiation map is a simplification made to allow an efficient update of the dose dispersed in the environment, which allows real-time decision-making during robot navigation. The main objective is to avoid demanding previous environment mapping and avoid restricting the operation to small spaces. Nonetheless, due to this simplification, information is lost about more complex obstacles, such as multiple surfaces at different heights but at the same x,y position. There is no way to get around this limitation without changing the map to some 3D environment representation; however, this could drastically increase the updating costs. Our strategy seeks to reduce this problem by making the robot disperse the maximum amount of UV-C dose on the borders of obstacles, covering the contour of the entire traversable area. Any areas where the robot
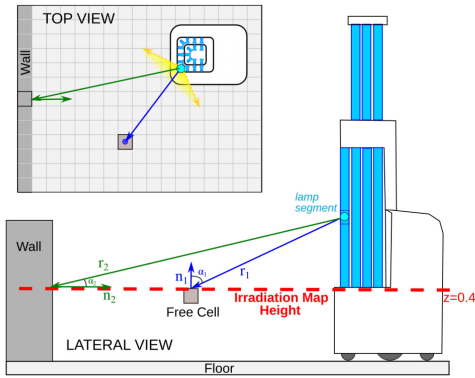
Fig. 2. The UV-C doses are computed at the height of the Irradiation Map plane. For simplification, the UV-C dose is calculated in the free space cells considering a vertical surface normal (parallel to the ground, tables, etc). In the border of free-space, the computation considers horizontal surface normals, simulating vertical obstacles like walls. The UV-C Dose of a given cell relative to a lamp is computed only if the cell is in its direct light field.
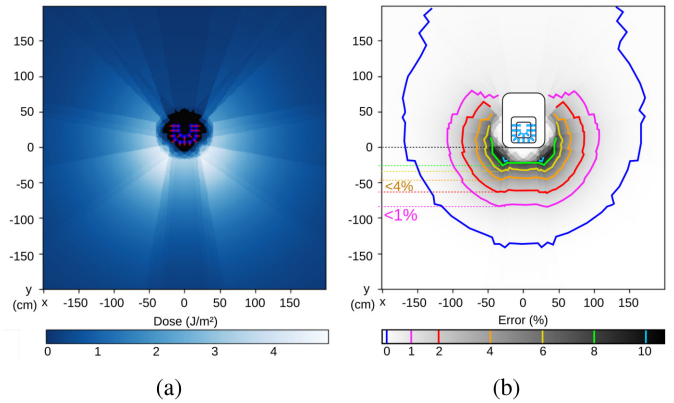

Fig. 3. Visualization of the lamps' irradiation for a lamp segmentation of 15 cm. (a) Shows the combined irradiation of the 18 lamps attached to our robot. (b) Shows the error in comparison with doses obtained with 1 cm segmentation. Farther than 1 m from the robot, the error is smaller than 1%.

Algorithm 1: Dose Calculation for Multiple Lamps.

1 **Initialization**;
2 **while** *lamps are on* **do**
3   **Compute time difference since last update**;
4   **for** *every visible cell around the robot* **do**
5   **for** *every lamp segment* **do**
6   **if** *cell is in the lamp's direct light field* **then**
7   **Get $\vec{r}$ from lamp segment to cell**;
8   **Increase cell's UV-C dose (use Eq. 4)**;
9   **end if**
10   **end for**
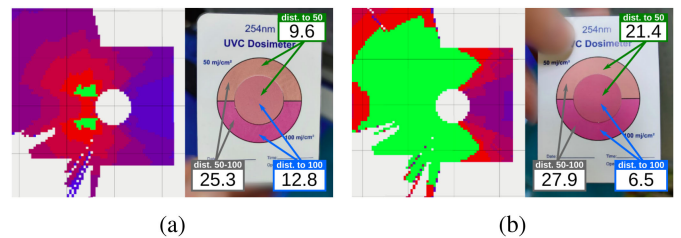11   **end for**
12 **end while**

Fig. 4. Analysis of the Irradiation Map in comparison to irradiation doses measured by UVC dosimeters. Irradiation maps of two tests, considering ideal dose of 50 mJ/cm^2, with disinfected regions in green. Next to each map, UVC dosimeters (placed at 50 cm in front of the robot) show the measured doses in each test. The numbers represent the color differences computed between each color indicator, using the CIELab ΔE distance metric.

cannot approach properly can be identified by the deficiency in the dose received (and if it is of interest, they can be signaled for a posterior cleaning process).

Given the mathematical model of the UV-C irradiation, Algorithm 1 computes the dose ξ that is delivered to each map cell. Each iteration of Algorithm 1 calculates the dose applied to the cells surrounding the robot. Initially, it computes the time difference since the last update. Then, we estimate the map cells that are visible to the robot, i.e. those not occluded by obstacles. Each cell is checked in relation to the position and orientation (transformed according to the current robot's pose) of every lamp, that is divided into multiple small segments, only updating the dose relative to lamps that have the cell within their direct light field. The lamps' maximum power and field of incidence are known beforehand, as well as their positions in the robot. The UV-C dose update follows (4).

The choice of height z of the Irradiation Map plane is configurable. For the most conservative estimate, we may compute the Irradiation Map at ground level, because by the time the cells at floor height reach the desired dose, higher cells (situated between the lamps and the floor) will have received more irradiation. This effect is stronger in the robot vicinity, where the difference in the

z axis greatly affects the final distance between cell and lamp. Higher heights, closer to the lamps, tend to reach the desired dose more quickly.

Another important point to be addressed refers to the level of segmentation that must be applied to each lamp. The smaller the size of each segment, the closer to the actual result the computed final dose will be. However, the update cost increases linearly with the number of lamp segments and can become prohibitive for real-time updates. After preliminary tests comparing different segmentation sizes with lamps segmented at every centimeter, we opted for segmentation every 15 cm. Fig. 3 presents the result of the Algorithm 1 for the Jaci lamps configuration, radiant flux $\phi_e = 12$ W, $\Delta t = 1$s and cells at $z = 0$ m. It shows an example of the resulting dose map considering such segmentation, in (a), and the error compared to the maximum segmentation, in (b). Note that regions farther than 50 cm away from the robot have an error smaller than 4%, dropping under 1% 80 cm away. When choosing the desired dose, it is normal to incorporate a margin of tolerance greater than such an error, thus this is not a critical problem.

Fig. 4 presents results of preliminary experiments carried out with the physical Jaci robot in an environment containing UVC

Dosimeters[1] to measure the UV-C irradiation. Such dosimeters are colorimetric indicators made of a sensitive material that after exposure to UV-C change colors (from yellow to orange to pink), demonstrating the accumulated dose of UV-C energy. Unfortunately, with the exception of the colors at the values of 50 and 100 mJ/cm^2, there is no accurate model of how the color changes along the irradiation accumulation. So, to get a measure of how close the value is to one or the other reference value, we compute the distance from the measured color to the other two colors in the CIELab color space[2].

For this test, we left the robot stationary in the environment, turned on all its UV-C lights, and positioned a UVC dosimeter 50 cm in front of the robot. As time passed, the Irradiation Map[3] was updated. The lamps were turned off after 130 seconds when the Irradiation Map showed that regions close to the robot began to reach the desired dose of 50 mJ/cm^2, as shown in green in Fig. 4(a). A second similar test was performed, this time keeping the lamps on for 191 seconds. This allowed the robot to disinfect a much larger region than in the previous test, as shown in Fig. 4(b). Analyzing the color difference values, we can see that in Fig. 4(a), the color was slightly closer to the low reference value, while in Fig. 4(b), it moved away from this value and got very close to the high reference value. Although a deeper analysis using more precise sensors is advisable to properly verify the quality of the implemented Irradiation model, the preliminary test is a good indication that the dose received was higher than the desired dose as indicated by the computed irradiation map.

III. Autonomous Disinfection Planner Based on the Irradiation Map

Although many UV-C disinfection approaches use a stationary light source, disinfection of distant regions is very slow because energy decays quadratically in terms of distance. In fact, as shown in other works [10], it is known that a mobile light source can disinfect faster than a stationary one.

With this in mind, we can argue that an autonomous robot has to fulfill some requirements to efficiently disinfect an environment thoroughly. Like humans, the robot should:

- Move as close as possible to the obstacle surfaces to maximize the UV-C irradiation on every obstacle;
- Visit all reachable free space in the environment, and perform exploration to gain more information;
- Evenly disinfect the environment, in which no free space remains infected;

- Be fully autonomous, deciding where to go and when the disinfection is done without human interference.

We propose a high-level planner that sequentially selects waypoints in an environment aiming to fulfill such requirements. Once waypoints are generated, the robot control can be adjusted by a local trajectory planning strategy, such as the one present in the standard ROS navigation stack. Our proposal uses as input a global 2D costmap that is initially empty but, as the robot moves, incrementally combines information of a traditional 2D SLAM map and 3D local data obtained by RGBD cameras, along with the Irradiation Map from Section II. We explain below how we addressed each requirement in our planner.

A. Moving Close to Obstacle Surfaces

The delivered UV-C energy is computed based on the distance between the light and the obstacle's regions, in which the closer the light is to the obstacle, the higher is the dose. Hence, the robot has to encircle the obstacles in the environment, respecting a distance range to the obstacle surfaces. If the robot gets too close to obstacles, it may crash into an obstacle. On the other hand, the delivered UV-C dose reduces if it gets too far from the obstacles.

In our planner, all the obstacles within our 2D gridmap are expanded λ cells towards the free space. The expansion size λ specifies the distance the robot should keep from the obstacles; it is defined as the smallest safest distance for which the robot will not collide, according to the robot's characteristics. Only the cells at the border between free space and such obstacle expansion are eligible to be selected as waypoints. Therefore, the robot will mainly move over such borders, and hence, it will avoid collisions and ensure the delivered UV-C will reach the obstacle surfaces with maximum efficiency.

B. Visiting All Reachable Environment

It is vital for the disinfection that the robot visits all reachable free spaces to maximize the object surfaces irradiated by the UV lights. Since the environment is initially unknown, the robot has to explore it to gain information and discover all the free and accessible regions. Thus, only the inaccessible regions to the robot would remain not fully disinfected at the end of the process.

Our planner fulfills the exploration requirement by making the robot move around the border of all obstacles that are still not disinfected. In short, the method selects an initial waypoint and proceeds to select neighboring waypoints in the same direction, until the entire course is completed. Note that even if the robot starts disinfecting in a given direction, the border cells left behind will be visited later after the robot circulates throughout the environment.

After completing the disinfection of an obstacle border, the method goes to the next obstacle with the nearest border not disinfected. Assuming there will be no obstacles farther apart than the robot's sensors range (i.e. one can always detect an obstacle from the vicinity of some other obstacle), every region

---

[1]UVC Dosimeters are made with a patented technology owned by Intellego Technologies. Research Institutes of Sweden (RISE) has validated and confirmed the products' photochromic material at various UV-C wavelengths (222 nm, 254 nm, 265 nm, and 278 nm) and has verified the color change at specific doses levels. Previous studies [13] showed that the UVC Dosimeter's color change from starting yellow to orange and deep pink correlated to a 3-log (99.9%) reduction of MRSA and C. Diff.

[2]CIELab is a color space designed to be perceptually uniform, that is, in which the numerical distance ΔE between two colors, [14], is proportional to the visual difference between them.

[3]For these tests, the Irradiation maps shown in Fig. 4 consider the maximum optical efficiency value at each point. As the dosimeters were directly facing the lamps, the optical efficiency of the UV irradiation was the maximum in the measured position.
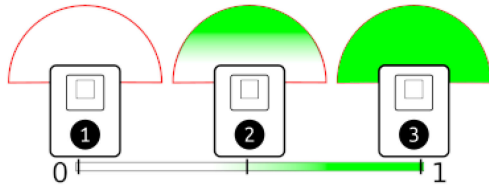
Fig. 5. Top-view examples of the β value in relation to the disinfected region within the semicircle in front of the robot.

Fig. 6. Example of disinfection in a simulated environment. Green cells are the ones in the reachable space that already received more than 100% of the desired UV-C dose in the initial passage through the environment.

of interest will be disinfected. In general, this assumption is valid[4] in environments such as rooms and offices.

C. Disinfecting the Environment Uniformly

The Irradiation Map built during the disinfection plays an important role in estimating the delivered UV-C dose. Our planner uses it to prevent the robot from wasting resources by disinfecting the same region multiple times. Besides, it exposes the regions that do not satisfy the ideal UV-C dose, helping the planner guide the robot throughout the environment to perform the disinfection consistently.

Consider, for example, a squared room and only a table in the center. The robot starts the disinfection next to the walls, and when it revisits its initial position, the dose map will indicate that the table region has a low UV-C dose. Then, our planner would guide the robot towards the table to continue the disinfection. Our planner repeats this process until there are no accessible obstacle surfaces lacking disinfection.

We assume that the low UV-C dose regions lack disinfection because we aim that the visited regions by the robot receive the ideal dose. The robot's speed is constantly computed to make sure the proper UV-C is delivered on the closest obstacle's surface. The current robot's speed, $\mathbf{r}_s$ is defined as

$$\mathbf{r}_s = \beta v, \tag{5}$$

in which v is the robot's maximum speed, in m/s. In this work, the $v = 0.1$ m/s. β is the speed factor that adjusts the current speed, and it ranges as $0 \leq \beta \leq 1$. To compute β, we first calculate the average dose, δ, within a semicircle in front of the robot's current pose. Then we compared it to the ideal dose to be delivered, i.e., $\beta = \delta / \xi$.

When the robot is in a fully disinfected region, as illustrated by the robot 3 in Fig. 5, $\delta \simeq \xi$. Hence, $\beta \simeq 1$, which makes the robot moves at its maximum speed. On the other hand, when the robot is in a region that has not been disinfected yet, robot 1 in Fig. 5, $\delta \simeq 0$. Then $\beta \simeq 0$, which makes the robot slow down to properly administer the dose at its surroundings.

D. Being Fully Autonomous

Combining our solutions to the previous requirements results in a fully autonomous robot for UV-C disinfection. The robot moves through the environment next to the border of obstacle, maintaining an ideal distance to them, as shown in the example

in Fig. 6. As the robot moves, it gains more information about the environment and simultaneously computes the dynamic Irradiation Map. Such a map estimates the delivered UV-C energy, and our planner uses it to decide whether the robot should slow down to irradiate more UV-C at its current position or go somewhere. Lastly, after the Irradiation Map indicates that the reachable cells are fully disinfected, our planner finishes the UV-C disinfection process. Therefore, the robot is able to decide when the disinfection is complete, and no human assistance is required.

IV. EXPERIMENTS

The experimental validation was made by comparing our proposal with different disinfection strategies in multiple simulated scenarios. The experiments were carried out using the Jaci robotic platform, developed by Instor [9], in the Gazebo simulation environment with ROS. All tested strategies used the traditional Gmapping technique[5] to solve SLAM and generate the 2D occupancy gridmap required by the Irradiation Map; they also used the Timed-Elastic-Band local planner[6] to guide the robot to the goals defined by the navigation strategies.

A. Different Disinfection Planners for an Autonomous Robot

Our proposal is compared[5] against three other[16] strategies that could be used as planners for autonomous disinfection. Each strategy is explained below, and next their results are compared to the ones from ours.

1) Fixed Speed Wall-Follower: It consists of the same trajectory generated for the proposed method: the robot moves on the border of the free space, following the walls/obstacles. However, it always maintains a fixed speed of 0.1 m/s during navigation, regardless of the dose deposited in the environment. The technique ends when the robot visits all reachable points around obstacles.

2) Sweeping Planner: Inspired by the navigation strategy applied to autonomous vacuum cleaners, the Sweeping planner makes the robot move through the environment in a zigzag pattern. The free space is sampled as a grid of equally-spaced points, and the robot visits one by one following the pattern. To ensure that the environment is properly disinfected, the robot

---

[4]If this is not the case, other problems will arise, such as the degradation of the SLAM process in zones with no measurements.

[5][Online]. Available: http://wiki.ros.org/gmapping
[6][Online]. available:http://wiki.ros.org/teb_local_planner

Scenario A

(a) Hospital Room   (b) Sweeping   (c) Voronoi   (d) Wall-Following

Scenario B

(e) Office   (f) Sweeping   (g) Voronoi   (h) Wall-Following

Scenario C

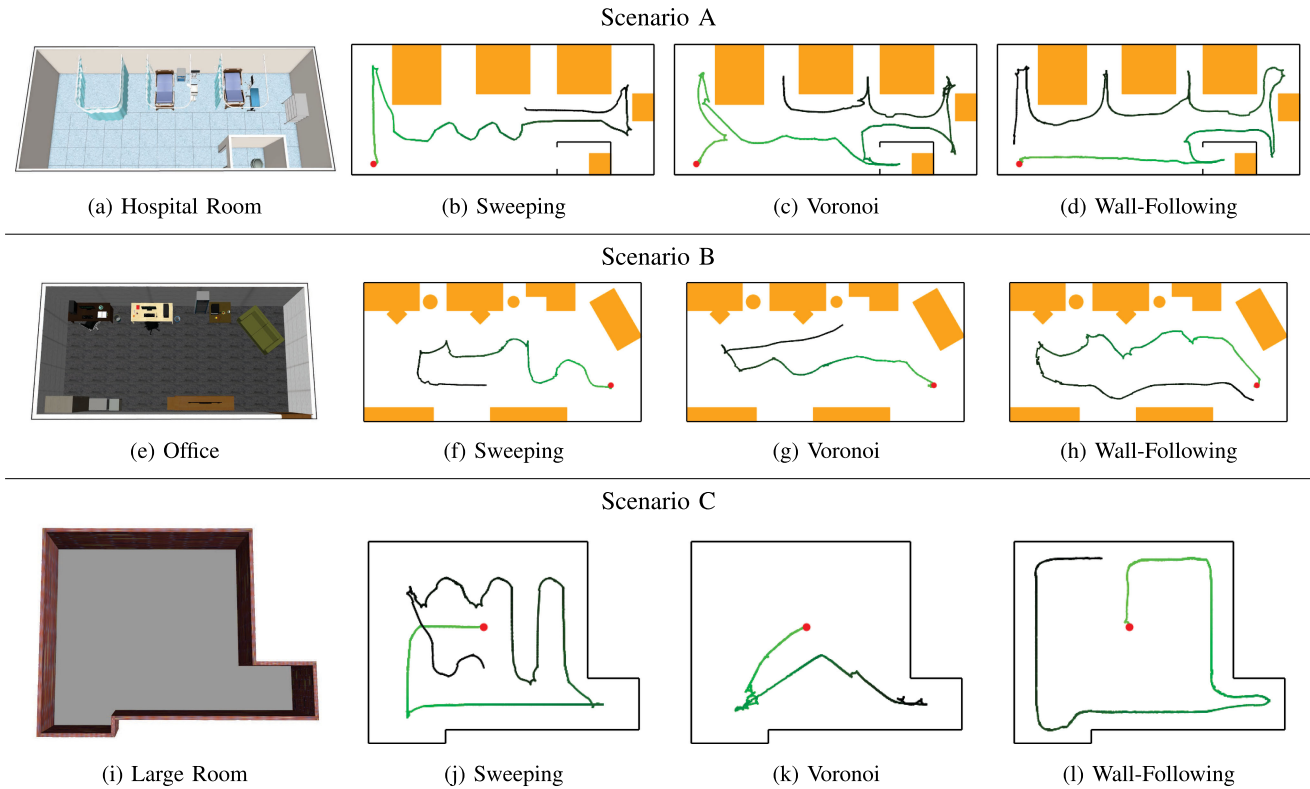(i) Large Room   (j) Sweeping   (k) Voronoi   (l) Wall-Following

Fig. 7. The three scenarios used in our experiments, followed by the paths generated by the methods of Sweeping, Voronoi-based, and our proposal in the experiments with high ideal dose. The paths shown are the ones with median performance across all tests for each configuration. The Hospital Room, depicted in (a), is a rectangular environment with a small bathroom and free space between objects. The Office in (e) is another rectangular environment, and most of its free space is in the center. Lastly, (i) shows the Large room, which is a large and empty environment.

remains stationary after reaching each local goal until the dose in the surroundings reaches the desired value (measured 50 cm ahead of the current point). The disinfection is performed while the robot moves through all points and it makes the robot cover most of the environment's free space.

3) Voronoi-Based Planner: Voronoi diagrams are a popular approach in the mobile robotics and computer vision research communities. In mobile robotics, they are widely used to compute the regions of a 2D gridmap that are equally distant from obstacles, making them the safest regions for the robot to traverse. Also, the Voronoi diagram generates a roadmap that passes through the center of all free regions of the environment, so it is commonly used as the basis for exploration methods. Here, the planner determines the closest Voronoi cell to the robot that has not been disinfected yet. When the robot reaches that cell, the robot waits until the region is properly disinfected (using the same strategy from the previous approach), and the process is repeated until no Voronoi cells remain infected. Despite its safety and efficiency in exploring the whole space, such a strategy fails to maintain the UV-C irradiation maximum to the obstacle surfaces in wide spaces.

B. Comparison of Different Disinfection Planners

Our experiments aim to measure the performance of the four planners while disinfecting three scenarios presented in Fig. 7.

The three rooms vary considerably: Scenario A - Hospital room (Fig. 7(a) - requires the robot to access narrow spaces whereas, Scenario B - Office (Fig. 7(e)) - is a smaller room with furniture arranged near the walls, and Scenario C - Large Room (Fig. 7(i)) - is completely empty. Fig. 7 also presents examples of the robot path generated by the sweeping, the Voronoi-based approach, and the wall-following strategy used by our proposal for each scenario.

We tested the planners considering two different doses of 20 mJcm/^{2} and 100 mJcm/^{2}, as if they were performing disinfection for a virus, such as the SARS-CoV-2, which requires small doses of UV-C to be eliminated [15], or for a bacteria, which requires higher UV-C doses [16], [17]. Every combination of planner, scenario, and ideal dose was repeated five times, totaling 120 experiments. It is also worth mentioning that every scenario has a fixed initial robot pose, regardless of planner or UV-C dose tested. Furthermore, as the robot's field-of-view only captures the front and side areas of the robot, before starting the navigation following the chosen planning strategy, the robot always performs a 360-degree turn to minimally map the grid around its initial position.

The planners' performance was evaluated in terms of the disinfection time, how much of the free space was disinfected, and how much of the space near obstacles were disinfected. Disinfecting the border of the free space, i.e. the space near the surfaces of the obstacles, is more effective to reduce the viruses

(a) Hospital Room 100 mJ/cm² (b) Office 100 mJ/cm² (c) Large Room 100 mJ/cm²

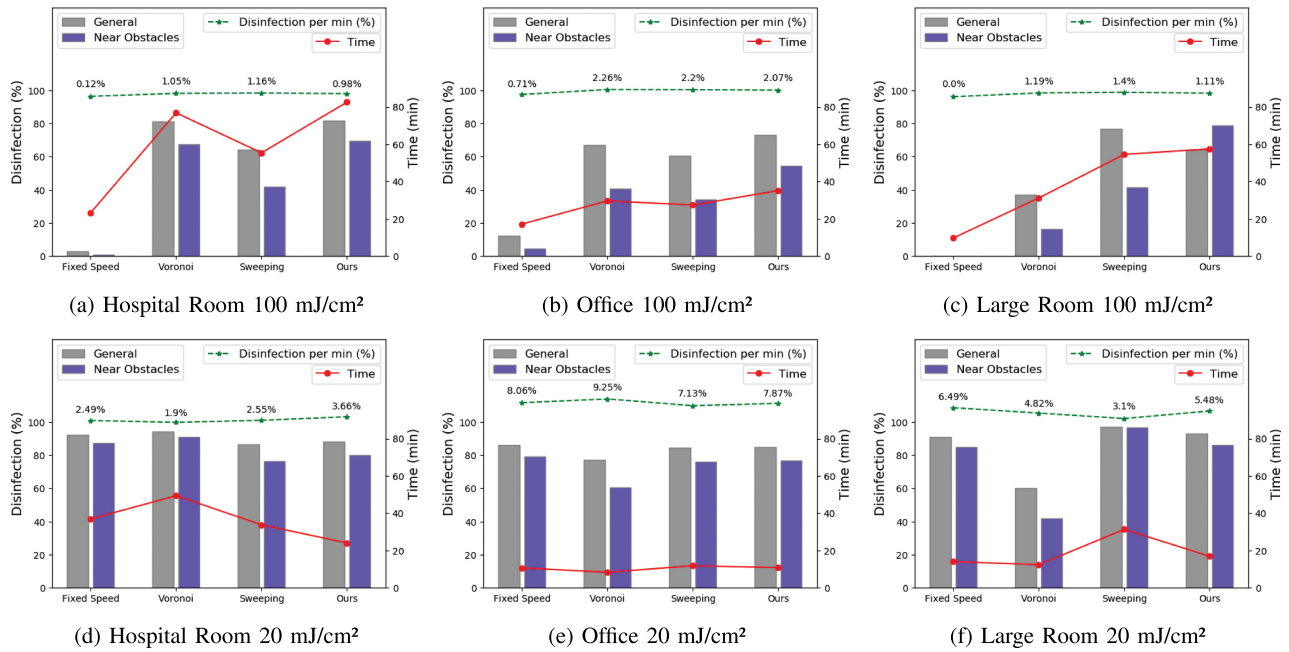(d) Hospital Room 20 mJ/cm² (e) Office 20 mJ/cm² (f) Large Room 20 mJ/cm²

Fig. 8. Comparison of total disinfection, disinfection time, and rate per minute obtained by all methods in each configuration.

spreading, different of disinfecting whole empty regions, which can take a long time and be less useful.

Fig. 8 shows the average disinfection rate of all free-space cells and the average disinfection rate of the cells near obstacles for all tested configurations. Additionally, Fig. 8 also presents the average disinfection times and the average disinfection rate per minute obtained by all methods in each configuration.

1) Disinfection With High Ideal UV-C Dose: When the desired dose is high, the decision of where to go and how to control the robot speed are fundamental factors to obtain good results. Simply exploring the environment with fixed speed without considering the required disinfection dose is clearly not a good strategy. Such a strategy quickly maps the entire environment, but the navigation made by the robot is too fast, and the lights end up staying on for not enough time to disinfect. The Voronoi-based strategy generally works well for covering the environment, except for wide areas. In such a case, as can be seen in the Large Room scenario (Fig. 7(k)), the robot only visits the center of the free space and the disinfection is impaired. In addition, the robot technique to stop and wait for the dose to reach the desired level worked well to disinfect the regions covered by the trajectory. The sweeping technique is able to achieve good disinfection rates, especially in open environments, where Voronoi-based one fails. On the other hand, its performance is worse in narrow areas, because the trajectory generated on top of a regular grid may not adequately cover such regions, as shown in the Hospital room (Fig. 7(b)) when the robot could not enter the space between the beds or pass through the door to the bathroom. Finally, the proposed technique controlling the speed dynamically obtained the best results in general.

In terms of disinfection rate per minute, the three techniques (apart from the fixed speed one) showed very similar results. This means that the final differences are mainly due to variations

in the disinfection time, depending on the trajectory length. It could be argued that it would be enough to give the same disinfection time to all methods, and the performance would be similar. In some way, this is true, but only if the chosen method covers the entire navigable area during that time, which is not always the case with the alternative strategies, as already discussed. On the other hand, it is a priori unknown how much time is needed to disinfect a specific environment, as this depends not only on its size but also on the arrangement of obstacles, so a method capable of adapting to different scenarios is quite advantageous. In this case, the proposed method was the one that best covered all types of environments.

As for the analysis of disinfection in areas near obstacles, the most challenging environments are those that have objects that prevent the robot from approaching them from all sides, such as sofas and tables near walls. In this type of situation, the robot ends up staying away from surfaces that could be disinfected if the furniture could be moved, such as the free spaces behind those objects. On the other hand, in places such as the Large Room, navigating near the walls makes the area more efficiently disinfected than the remaining space. As shown in Fig. 8(c), the percentage of the disinfected area near obstacles (purple bars) almost doubled from the Sweeping method to the proposal while maintaining similar disinfection times.

2) Disinfection With Low Ideal UV-C Dose: In general, the disinfection rate is much higher when the desired dose is low (Fig. 8(d)–(f)). Regardless of the planner chosen, the simple fact of moving through the environment with the lights on generates enough UV-C energy to disinfect a large part of the place. If the environment has mainly narrow regions, all techniques work well. However, in wider spaces, the Voronoi-based approach stays too far from the walls thus obtaining small disinfection rates (Fig. 8(f)). The fixed speed strategy obtained very good

results in all scenarios. This happens because a robot moving with a fixed regular speedcan quickly spread low UV-C doses even over long distances, basically disinfecting everything in its surroundings while moving.

Interestingly, despite similar disinfection times, the proposed wall follower with speed control was faster than its fixed speed counterpart in the Hospital scenario. An explanation is that the fixed speed strategy visits all possible regions, even those wholly disinfected. In contrast, yet another advantage of the proposed approach is that it easily detects and skips already-disinfected areas from afar, reducing trajectory length.

V. Conclusion

This letter presented an autonomous UV-C disinfection strategy for indoor environments based on a dynamic Irradiation Map, that indicates the amount of energy applied in each region of the environment. The approach was evaluated in multiple simulated scenarios in comparison to other planning techniques. The main contributions of the letter are:

- A 2D irradiation mapping technique that works for arbitrarily desired UV-C doses, while considering light sources in the 3D space;
- A high-level planning strategy that guides the robot autonomously in the environment, trying to cover all regions containing obstacles with UV-C light;
- A speed control for the planner that adapts dynamically according to the energy dose in the irradiation map;
- A detailed analysis of how different values of desired dose affect the way navigation can be efficiently done.

An important point observed in the experiments is that the lower the amount of energy needed for disinfection, the less critical is the choice of navigation method (given that, at some point, the robot covers all the space that it wants to disinfect). Still, with higher dose values, the choice of where the robot should go and the speed control based on the Irradiation Map is fundamental for the disinfection to work properly.

However, it must be clear that it is not possible to guarantee complete disinfection of the environment using only UV-C light. The robot will always be limited in terms of navigation by the configuration of obstacles in the environment, and the obstacles also generate occlusions for the light sources. Even so, in that situation, the Irradiation Map can be used to indicate regions that still need manual disinfection. Also, we perform several simplifications, like working with a 2D map, that makes us lose information about the environment, but such simplifications are necessary to allow efficient performance in different scenarios and real-time decision-making while the map is being discovered.

As future work, we are precisely investigating the combination of other disinfection techniques to be carried out in conjunction with UV-C lighting. Furthermore, in view of the obtained results, it is possible to investigate the best way to disinfect an environment given time constraints (for example, when the periods in which a room will be empty are very short). Finally, another idea currently being pursued is to measure the effectiveness of the proposed strategy in controlled environments containing pathogens, which would be the best possible experimental validation of our approach.

References

[1] J. Zhang, G. Lin, J. Zeng, J. Lin, J. Tian, and G. Li, "Challenges of SARS-CoV-2 and lessons learnt from SARS in Guangdong province, China," *J. Clin. Virol.*, vol. 126, 2020, Art. no. 104341.
[2] G. Kampf, D. Todt, S. Pfaender, and E. Steinmann, "Persistence of coronaviruses on inanimate surfaces and their inactivation with biocidal agents," *J. Hosp. Infection*, vol. 104, 3, pp. 246–251, 2020.
[3] N. van Doremalen *et al.*, "Aerosol and surface stability of SARS-CoV-2 as compared with SARS-CoV-1," *New England J. Med.*, vol. 382, no. 16, pp. 1564–1567, 2020.
[4] S. Wu, Y. Wang, X. Jin, J. Tian, J. Liu, and Y. Mao, "Environmental contamination by SARS-CoV-2 in a designated hospital for coronavirus disease 2019," *Amer. J. Infection Control*, vol. 48, no. 8, pp. 910–914, 2020.
[5] S. W. X. Ong *et al.*, "Air, surface environmental, and personal protective equipment contamination by severe acute respiratory syndrome coronavirus 2 (SARS-CoV-2) from a symptomatic patient," *JAMA*, vol. 323, no. 16, pp. 1610–1612, 2020.
[6] D. J. Anderson *et al.*, "Enhanced terminal room disinfection and acquisition and infection caused by multidrug-resistant organisms and clostridium difficile (the benefits of enhanced terminal room disinfection study): A cluster-randomised, multicentre, crossover study," *Lancet*, vol. 389, no. 10071, pp. 805–814, 2017.
[7] A. R. Marra, M. L. Schweizer, and M. B. Edmond, "No-touch disinfection methods to decrease multidrug-resistant organism infections: A systematic review and meta-analysis," *Infection Control Hosp. Epidemiol.*, vol. 39, no. 1, pp. 20–31, 2018.
[8] H. Kitagawa *et al.*, "Effectiveness of 222-nm ultraviolet light on disinfecting SARS-CoV-2 surface contamination," *Amer. J. Infection Control*, vol. 49, no. 3, pp. 299–301, 2021.
[9] "Instor robotics and projects," Accessed: Sep. 09, 2021. [Online]. Available: https://www.instor.com.br/projeto/9
[10] L. Tiseni, D. Chiaradia, M. Gabardi, M. Solazzi, D. Leonardis, and A. Frisoli, "UV-C mobile robots with optimized path planning: Algorithm design and on-field measurements to improve surface disinfection against SARS-CoV-2," *Robot. Automat. Mag.*, vol. 28, no. 1, pp. 59–70, 2021.
[11] P. Chanprakon, T. Sae-Oung, T. Treebupachatsakul, P. Hannanta-Anan, and W. Piyawattanametha, "An ultra-violet sterilization robot for disinfection," in *Proc. Int. Conf. Eng., Appl. Sci. Technol.*, 2019, pp. 1–4.
[12] D. Conte, S. Leamy, and T. Furukawa, "Design and map-based teleoperation of a robot for disinfection of COVID-19 in complex indoor environments," in *Proc. IEEE Int. Symp. Saf., Secur., Rescue Robot.*, 2020, pp. 276–282.
[13] J. Cadnum, A. Jencson, S. Redmond, T. S. C. Mana, and C. Donskey, "1215. ultraviolet-C (UV-C) monitoring made ridiculously simple: UV-C dose indicators for convenient measurement of UV-C dosing," in *Open Forum Infectious Diseases*, 2019, vol. 6, no. Suppl 2, p. S437.
[14] M. R. Luo, G. Cui, and B. Rigg, "The development of the CIE 2000 colour-difference formula: CIEDE2000," *Color Res. Appl.*, vol. 26, no. 5, pp. 340–350, 2001.
[15] M. Biasin *et al.*, "UV-C irradiation is highly effective in inactivating SARS-CoV-2 replication," *Sci. Rep.*, vol. 11, no. 1, pp. 1–7, 2021.
[16] W. Hijnen, E. Beerendonk, and G. Medema, "Inactivation credit of UV radiation for viruses, bacteria and protozoan (OO)cysts in water: A review," *Water Res.*, vol. 40, no. 1, pp. 3–22, 2006.
[17] M. Masjoudi, M. Mohseni, and J. R. Bolton, "Sensitivity of bacteria, protozoa, viruses, and other microorganisms to ultraviolet radiation," *J. Res. Nat. Inst. Standards Technol.*, vol. 126, pp. 1–77, 2021.